Applied Physics Letters

Gate-induced switching of perpendicular exchange bias with very low coercivity in Pt/Co/Ir/Cr_2O_3/Pt epitaxial film

Cite as: Appl. Phys. Lett. **122**, 062404 (2023); https://doi.org/10.1063/5.0131695
Submitted: 23 October 2022 • Accepted: 23 January 2023 • Published Online: 08 February 2023

Hirofumi Ekawa, Jiaqi Shen, Kentaro Toyoki, et al.

Applied Physics Letters ARTICLE scitation.org/journal/apl

Gate-induced switching of perpendicular exchange bias with very low coercivity in Pt/Co/Ir/Cr_2O_3/Pt epitaxial film

Cite as: Appl. Phys. Lett. **122**, 062404 (2023); doi: 10.1063/5.0131695
Submitted: 23 October 2022 · Accepted: 23 January 2023 ·
Published Online: 8 February 2023

Hirofumi Ekawa,[1] Jiaqi Shen,[1] Kentaro Toyoki,[1,2,3] Ryoichi Nakatani,[1,2,3] and Yu Shiratsuchi[1,2,3,a)]

AFFILIATIONS

[1]Department of Materials Science and Engineering, Graduate School of Engineering, Osaka University, Suita, Osaka 565-0871, Japan
[2]Spintronics Research Network Division, Institute for Open and Transdisciplinary Research Initiatives, Osaka University, Yamadaoka 2-1, Suita, Osaka 565-0871, Japan
[3]Center for Spintronics Research Network, Graduate School of Engineering Science, Osaka University, Machikaneyama 1-3, Toyonaka, Osaka 560-8531, Japan

Note: This paper is part of the APL Special Collection on Magneto-ionic and electrostatic gating of magnetism: Phenomena and devices.
[a)]**Author to whom correspondence should be addressed:** shiratsuchi@mat.eng.osaka-u.ac.jp

ABSTRACT

We investigate magnetoelectric switching of perpendicular exchange bias with very low coercivity in a Pt/Co/Ir/Cr_2O_3/Pt epitaxial film. We also optimize the suitable Ir spacer thickness so that the film exhibits the perpendicular exchange bias greater than the coercivity up to the vicinity of the Néel temperature. Main impact of the Ir spacer layer is the significant reduction of coercivity less than 0.5 mT in maintaining both the perpendicular magnetic anisotropy and the perpendicular exchange bias. For the suitable structure, the perpendicular exchange bias was isothermally switched by the gate voltage in combination with the magnetic field. Analysis of the hysteresis of the exchange bias field as a function of the gate voltage suggested that the magnetoelectric coefficient was comparable to the reported value. This implies that the Ir layer does not degrade the efficiency to transfer the magnetoelectrically controlled antiferromagnetic order parameter to the ferromagnetic Pt/Co/Ir trilayer.

Antiferromagnetic (AFM) materials are recognized as materials wherein the magnetic moments are fully compensated, and hence, no net magnetization is emerged. Main use of AFM materials has been to fix the magnetization direction of the ferromagnetic (FM) layer in the magnetoresistive devices,[1] known as the exchange bias (EB).[2,3] Main requirements for EB are strength and direction; the EB field greater than the coercivity is desirable and should be directed to the surface normal. There are several approaches to meet these requirements, such as the control of AFM order parameter[4] and the magnetic nanostructure.[5] The tuning interfacial exchange coupling J by inserting the non-magnetic metal layer between FM and AFM layers is one of the direct ways. Attempts have been done for various systems, such as CoFe/Cu/IrMn,[6] Co/Cu/CoO,[7] Fe/Ag/CoO,[8] NiFe/(Cu, Cr)/NiO,[9,10] and NiFe/(Cu, Ag, Au)/CoO,[11] and revealed an intriguing effect of the nonmagnetic spacer layer on EB such as the exponential decay accompanied with/without oscillation as a function of spacer layer thickness.[10,11] In addition to the huge efforts for the in-plane exchange-biased system, the tuning of perpendicular exchange bias (PEB), which is more important in the modern spintronics, is an ongoing issue.[12] The perpendicular magnetic anisotropy (PMA) is induced at the heavy metal/3d FM layer, which can increase H_C due to the strong spin–orbit interaction of the heavy metal layer. In addition, the emergence of EB sometimes accompanies with the enhancement of H_C,[13] and thus, the suppression of H_C enhancement in the PEB system is non-trivial. Furthermore, as a main function of the conventional EB, a stabilization of FM magnetization direction relies on the robustness of the AFM spin against the magnetic field perturbation, meaning that the conventional EB is a passive effect. In contrast, the recent development of AFM spintronics[14] aims at the active control of the AFM spin/domain state and manipulating sign of EB in an isothermal way is going to be possible.[15–17] This renewal retrieves the pursuit of tuning J for the switchable PEB.

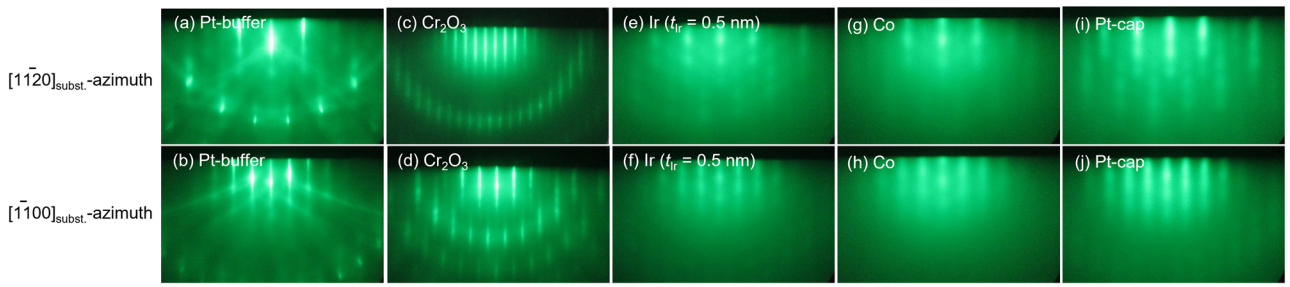

FIG. 1. RHEED images of (a) and (b) Pt buffer, (c) and (d) Cr_2O_3, (e) and (f) Ir, (g) and (h) Co, and (i) and (j) Pt capping layer for the film with $t_{Ir} = 0.5$ nm. Electron azimuths are [11$\bar{2}$0] and [1$\bar{1}$00] of the substrate for the top and the bottom panels, respectively.

The Pt/Co/spacer/Cr_2O_3(0001) system exhibits the PEB[18] switchable by the combination of magnetic and electric fields via the magnetoelectric (ME) effect.[19,20] On switching PEB, J to cause PEB affects the switching energy condition,[21,22] and thus, the fine tuning of J is required. The influence of the nonmagnetic spacer layer on PEB in this system was reported using Pt,[23] Cr,[16] and Au.[23,24] In the case of Pt, although FM and AFM layers were epitaxially grown, the H_C enhancement was significant.[23] Although Cr and Au could suppress the H_C enhancement, the shape of the magnetic hysteresis loop degrades, i.e., the low squareness probably because of the dispersion of the magnetic easy direction due to the non-epitaxial growth.[16,24] In this paper, we adopt Ir as a spacer material and investigate the influence on PEB and the H_C enhancement. We demonstrate the reversible switching of PEB by the gate voltage in combination with magnetic field using the suitable Ir layer thickness.

Pt(2.0 nm)/Co(0.5 nm)/Ir(t_{Ir})/Cr_2O_3(130 nm)/Pt(20 nm) film was fabricated on the α-Al_2O_3(0001) substrate by DC magnetron sputtering. After cleaning the substrate ultrasonically using acetone, methanol, distilled water, and isopropanol, it was heated in the vacuum chamber at 873 K. The 20-nm thick Pt buffer layer was formed at 873 K. The Cr_2O_3 layer was deposited on the Pt buffer layer at 773 K by sputtering of a pure Cr target in a mixture of Ar and O_2 gases. Ir, Co, and Pt layers were subsequently deposited at room temperature using the pure Ar. t_{Ir} was varied from 0 to 2.0 nm. The growth direction and the crystalline quality were evaluated by the *in situ* reflection high-energy electron diffraction (RHEED) and the *ex-situ* X-ray diffraction (XRD). RHEED observations were carried out for each surface. XRD measurements were carried out using the Cu K_α irradiation with the Ge(220) × 2 monochromator.

Magnetic properties were characterized by using vibrating sample magnetometer (VSM), magneto-optic Kerr effect (MOKE) magnetometry, and anomalous Hall effect (AHE) measurements. Saturation magnetization per unit area $M_S \cdot t_{FM}$ and the effective uniaxial magnetic anisotropy energy density $K_{eff} \cdot t_{FM}$ were evaluated based on the magnetization curves (M–H curves) measured by VSM. For these measurements, the magnetic field was applied to the direction perpendicular and parallel to the film. $K_{eff} \cdot t_{FM}$ was evaluated as

$$K_{eff} \cdot t_{FM} = \left(\int_0^{M_S \cdot t_{FM}} \mu_0 H dM t_{FM} \right)_{H//Film} - \left(\int_0^{M_S \cdot t_{FM}} \mu_0 H dM t_{FM} \right)_{H \perp Film}. \quad (1)$$

In this definition, the positive $K_{eff} \cdot t_{FM}$ corresponds to PMA. For the precise measurement of the low H_C ($\mu_0 H_C < 25$ mT) along the magnetic easy axis, the M–H curve was measured by using a Helmholtz

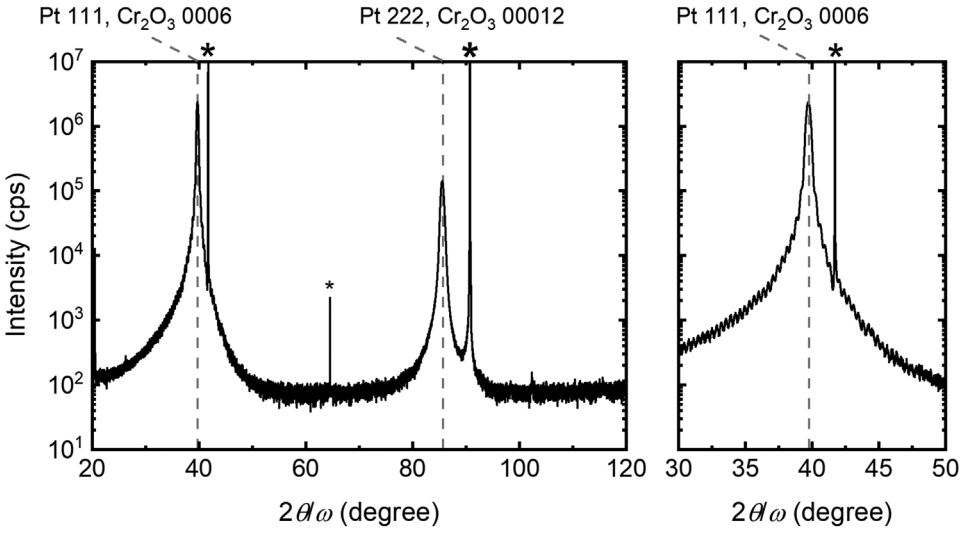

FIG. 2. XRD profile for the film with $t_{Ir} = 0.5$ nm. Right represents the enlarged profile around the diffraction from Pt(111)/Cr_2O_3(0006). The asterisk in the profile represents the diffractions from the substrate.

coil with the sweep speed of the magnetic field of 0.05 mT/s. Measurement temperature was room temperature (~296 K).

The MOKE measurements were carried out with the polar configuration where the magnetic field direction was perpendicular to the film. The wavelength of the light was 405 nm. The incidence angle was 10° from the surface normal. Measurement temperature of MOKE was varied from 80 to 300 K. On cooling, the magnetic field ($\mu_0 H = +0.4$ T) was applied.

ME switching experiment of PEB was done using the micro-Hall device with the 5 μm width and 25 μm length. Device was fabricated by photolithography and Ar ion milling. The device structure is similar to that used in Ref. 21. Measurement sequence is as follows. In these measurements, the magnetic- (H) and electric (E) field directions were perpendicular to the film. The positive direction of fields was defined as the direction from bottom to top of the film.

(1) Gate voltage V_G was applied across the Cr_2O_3 layer. In maintaining V_G, the high magnetic field $\mu_0 H = +5.5$ T was applied. The simultaneous application of V_G (E) and H is essential for the ME induced switching because the driving force by the ME effect is proportional to the EH product.[19,20]
(2) After (1), the AHE loop was measured in the weak field range of ±500 mT to check the PEB polarity.

(1) and (2) were repeated in sequentially varying V_G ranging from −5.0 to +10 V. We confirmed that the AHE loop did not change by $\mu_0 H = +5.5$ T alone. More details of the ME switching measurements can be found in our previous paper.[20]

Prior to show the ME switching results, we show the impact of the Ir spacer layer on PMA, H_C, and PEB to select the suitable t_{Ir} for the ME investigation. Figure 1 shows the RHEED images for each layer. The RHEED images of the Pt buffer layer and the Cr_2O_3 surface are streaky. The spacings of the streaks are equal. The diffraction

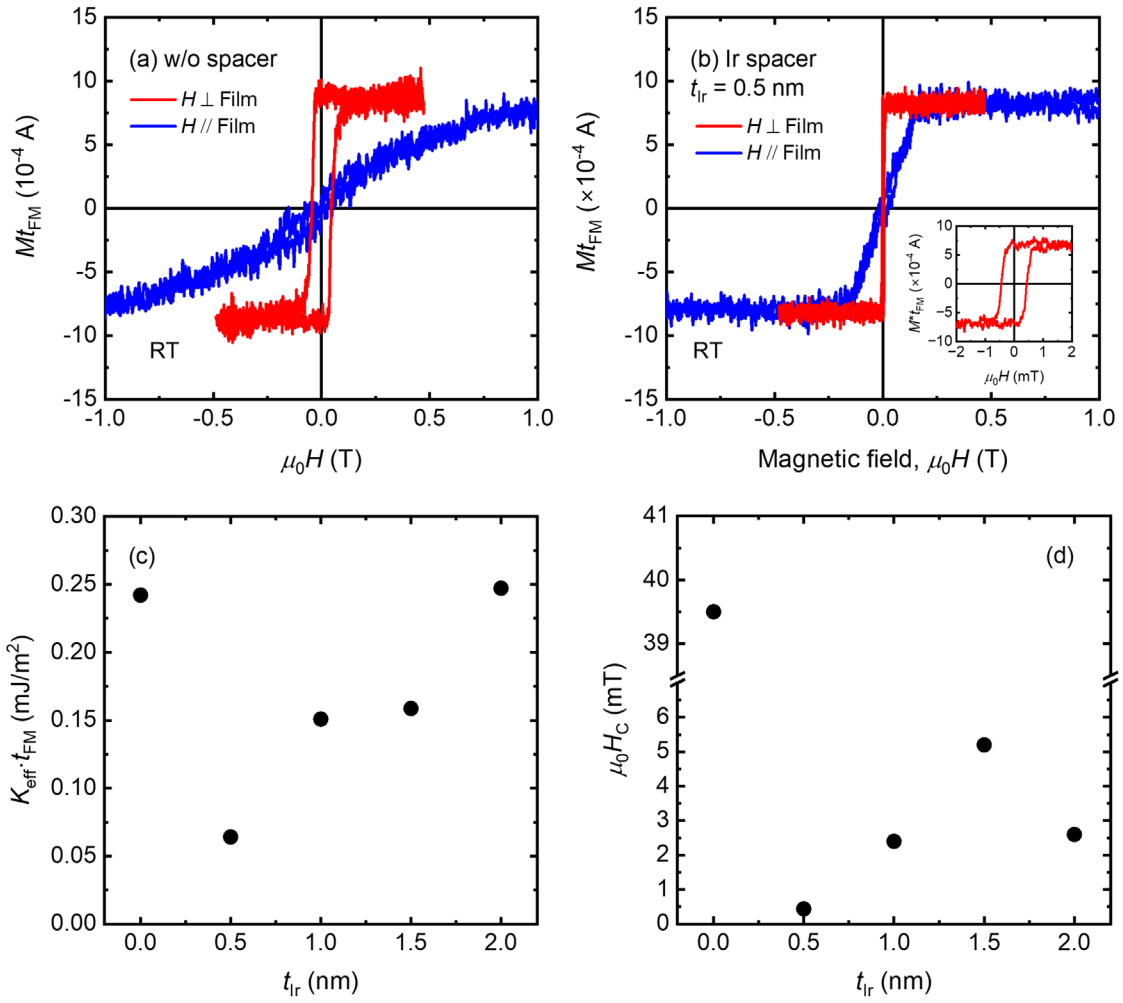

FIG. 3. Magnetization curves measured at room temperature. t_{Ir} is (a) 0 and (b) 0.5 nm, respectively. Red and blue curves show the curves for the field direction perpendicular and parallel to the film, respectively. The inset of (b) shows the enlarged curve for the direction perpendicular to the film measured using the Helmholtz coil. Data for other t_{Ir} are shown in the supplementary material. (c) and (d) represent the t_{Ir} dependence of $K_{eff} \cdot t_{FM}$ and $\mu_0 H_C$, respectively.

pattern indicates that the Pt buffer layer and the Cr_2O_3 layer form fcc(111) and corundum(0001), respectively, with the epitaxial relationship of Pt(111)[11$\bar{2}$]//Cr_2O_3(0001)[1$\bar{1}$$\bar{2}$0] in agreement with previous reports. The first Laue zone is also observed indicating the good crystalline quality. The RHEED images for Ir, Co, and Pt capping layers are similar to Figs. 1(a) and 1(b) except for the broadening of streaks and the absence of the first Laue zone. Thus, Ir, Co, and Pt capping layers are also epitaxially grown, and the epitaxial relationship is same as the above. The similar RHEED images were obtained for every t_{Ir}. In the XRD profiles ($2\theta/\omega$ profiles) shown in Fig. 2, the diffraction peaks from Pt(*lll*), Cr_2O_3(000*l*), and substrate were observed. Around the diffractions from Pt(111) and/or Cr_2O_3(0006), the Laue fringes are observed. The oscillation period corresponds to the Pt buffer layer thickness. Note that the diffractions from Pt(111) [Pt(222)] and Cr_2O_3(0006) [Cr_2O_3(00012)] are difficult to be distinguished because of the close lattice spacings.

Figure 3 shows the M–H curves measured at room temperature. The rectangular hysteresis loop is observed in the field direction perpendicular to the film, whereas the magnetization linearly increases or shows the S-shape until the saturation. Figure 3(c) shows the change in $K_{eff} \cdot t_{FM}$ with t_{Ir}. For every t_{Ir}, $K_{eff} \cdot t_{FM}$ is positive and all studied films shows PMA. With increasing t_{Ir}, $K_{eff} \cdot t_{FM}$ first decreases and recovers at $t_{Ir} = 2.0$ nm. The $K_{eff} \cdot t_{FM}$ values are comparable to the reported values in the Pt/Co(0.5 nm)/Ir multilayer.[26] We found $\mu_0 H_C$ along the direction perpendicular to the film, was very low (0.44 mT for $t_{Ir} = 0.5$ nm) whereas $\mu_0 H_C$ for $t_{Ir} = 0$ nm is about 40 mT. As shown in Fig. 3(d), the reduction of $\mu_0 H_C$ is common in every t_{Ir}. $\mu_0 H_C$ seems not to be correlate with $K_{eff} \cdot t_{FM}$. To obtain more insight of the low H_C, we compared $\mu_0 H_C$ with the case of the Pt spacer, Pt(2)/Co(0.5)/Pt(0.5)/Cr_2O_3(130)/Pt(20) which has the epitaxial relationship similar to the mainly used films. $\mu_0 H_C$ for the Pt spacer film was about 14 mT (see the supplementary material), higher than the Ir spacer system. We are aware of that the coercivity depends on the sweep speed of the magnetic field because the hysteresis is a time-dependent phenomenon. We confirmed that $\mu_0 H_C$ maintains the low value, 0.54 mT at 0.1 mT/sec. $M_S \cdot t_{FM}$ was $(7.0–7.5)\times10^{-4}$ A which is almost same as the bulk Co. $M_S \cdot t_{FM}$ can be higher than the bulk Co due to the induced magnetic moment of Pt.[24–28] Compared with other

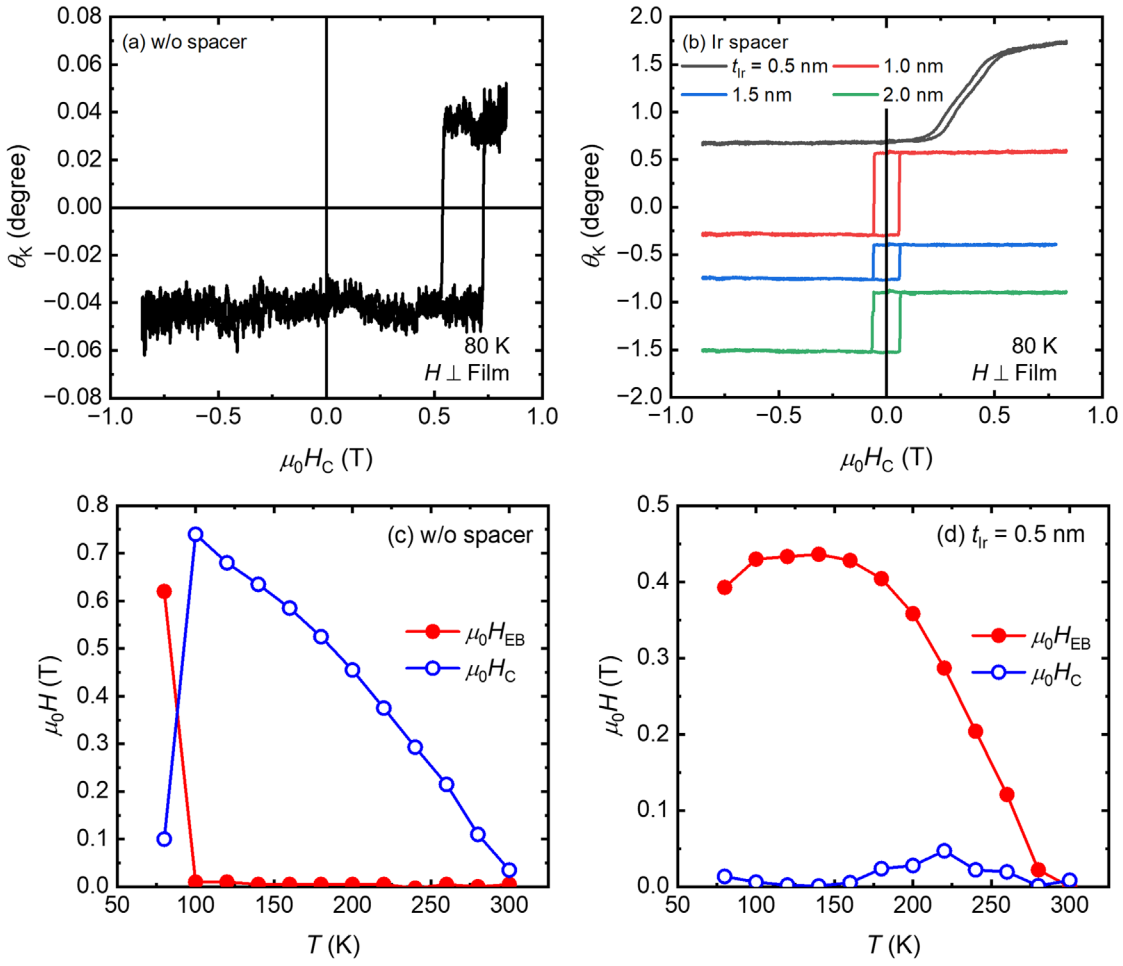

FIG. 4. (a) and (b) represent the polar MOKE loops measured at 80 K. t_{Ir} is (a) 0, (b) 0.5 (black), 1.0 (red), 1.5 (blue), and 2.0 (green) nm. (c) and (d) represent the temperature dependences of $\mu_0 H_{EB}$ and $\mu_0 H_C$ for (c) $t_{Ir} = 0$ and (d) 0.5 nm, respectively. Data for other t_{Ir} are shown in the supplementary material.

FM/Pt systems,[27,28] the enhancement of $M_S.t_{FM}$ is tiny probably because the spin-polarization of Ir is weaker than that of Pt.[29]

PEB was not observed at room temperature because of the Néel temperature T_N of the 130-nm thick Cr_2O_3 (~287 K[30]) lower than room temperature. By cooling the sample below T_N in the presence of magnetic field, PEB was observed. Figure 4 shows the polar MOKE loops measured at 80 K after the field-cooling. The films with $t_{Ir} = 0$ and 0.5 nm exhibit PEB [Figs. 4(a) and black curve in 4(b)]. The PEB field, $\mu_0 H_{EB}$ decreases with increasing t_{Ir} due to the short-range nature of J. The loop is gradual for $t_{Ir} = 0.5$ nm probably because the highest applied field is insufficient to saturate the magnetization. MOKE loops for $t_{Ir} \geq 1.0$ nm are the similar shape and does not show PEB.

Figures 4(c) and 4(d) show the temperature dependences of $\mu_0 H_{EB}$ and $\mu_0 H_C$. As seen in Fig. 4(c), for $t_{Ir} = 0$ nm, $\mu_0 H_{EB}$ disappears at 100 K, accompanying with the enhancement of $\mu_0 H_C$. The abrupt changes in H_{EB} and H_C agree with the previous report and is explained by the energetic competition between J and the magnetic anisotropy energy of the AFM layer.[18,23] For $t_{Ir} = 0.5$ nm, $\mu_0 H_{EB}$ survived above 280 K. The increase in the blocking temperature upon weakening J is explained in the above-mentioned framework. It is remarkable that the H_C enhancement is suppressed in the whole studied temperature regime. We previously reported that the Au space layer could suppress the H_C enhancement in the PEB system.[24] In the case of the Au spacer layer, H_C increased with increasing temperature, which is contrastive to the Ir spacer system. According to the phenomenological interpretation of EB based on the Meiklejohn and Bean model,[31] the H_C enhancement is attributed to the AFM spin rotation together with the FM magnetization reversal. In the presence of the distribution of the switching energy barrier of the AFM moment,[32] for example, caused by the size distribution, the small grain causes the H_C enhancement, and the large grain causes EB due to the pinned AFM moment. The low H_C below T_N should be attributed to the small switching energy dispersion of the AFM layer. For $t_{Ir} \geq 1.0$ nm, $\mu_0 H_{EB}$ was zero. Three films show the similar $\mu_0 H_C$ in the whole temperature regime indicating the decoupling of Pt/Co and Cr_2O_3. Details on M–H curves and MOKE for $t_{Ir} \geq 1.0$ nm are shown in the supplementary material.

Based on the results in Figs. 3 and 4, the film with $t_{Ir} = 0.5$ nm was used for the following ME investigation as the suitable structure. Figure 5(a) shows the AHE loop measured at 280 K, $T/T_N = 0.975$ after the field-cooling. The loop shifts to the negative H direction due to the positive cooling field. $\mu_0 H_{EB}$ is about −20 mT, yielding the exchange anisotropy energy density J_K ($= M_S \cdot t_{FM} \cdot \mu_0 H_{EB}$) of 0.015 mJ/m^2. Starting from the negative EB state, the positive ME field, i.e., the positive V_G and H was applied. Figure 5(b) shows the AHE loops after applying $V_G = +7.0$, 8.0, and 10 V in combination with $\mu_0 H = +5.5$ T. At $V_G = +7.0$ V, the loop shows the stepwise increase with increasing H. The step in the positive H regime gets deeper with increasing V_G, and finally, the loop settles into a fully positive PEB state. The stepwise increase has been observed in the double PEB state after the zero-field cooling[33,34] and in the intermediate state of the ME-induced switching process.[21,22] The similar change is observed in the positive to negative switching branch [Fig. 5(c)]. In this branch, the stepwise loops are observed in the V_G range of −3.0 V to −5.0 V. In both switching branches, H_C maintains the low value and the remarkable change is not observed. Note that the leakage current at the highest V_G (+10 V) was about 10^3 A/m^2 (not shown), sufficiently low to rule out the current-induced mechanism, such as spin–orbit torque.[35]

In the double exchange-biased loop with the stepwise increase, the remanence ratio M_R/M_S is relevant to the area ratio of positive and negative PEB regimes. Figures 5(d) and 5(e) show the changes in M_R/M_S and $\mu_0 H_{EB}$ as a function of V_G. Two curves show the hysteresis corresponding to the AFM domain switching. The coercive voltage V_{G_C} is asymmetric, and the hysteresis shifts to the positive V_G direction. The asymmetry in V_{G_C} is due to the unidirectional nature of the exchange anisotropy. Using V_{G_C}, J_K can be expressed as

$$J_K = M_S t_{FM} \mu_0 H_{EB} = \frac{\alpha \Delta E_C t_{AFM} H}{2}, \quad (2)$$

where α is the ME susceptibility, ΔE_C ($= V_{G\_C}/t_{AFM}$) is a difference in the coercive electric field in Fig. 5(d), and t_{AFM} is an AFM layer thickness. The first expression is the conventional definition of J_K and allows us to estimate J_K as mentioned above (0.015 mJ/m^2). The first

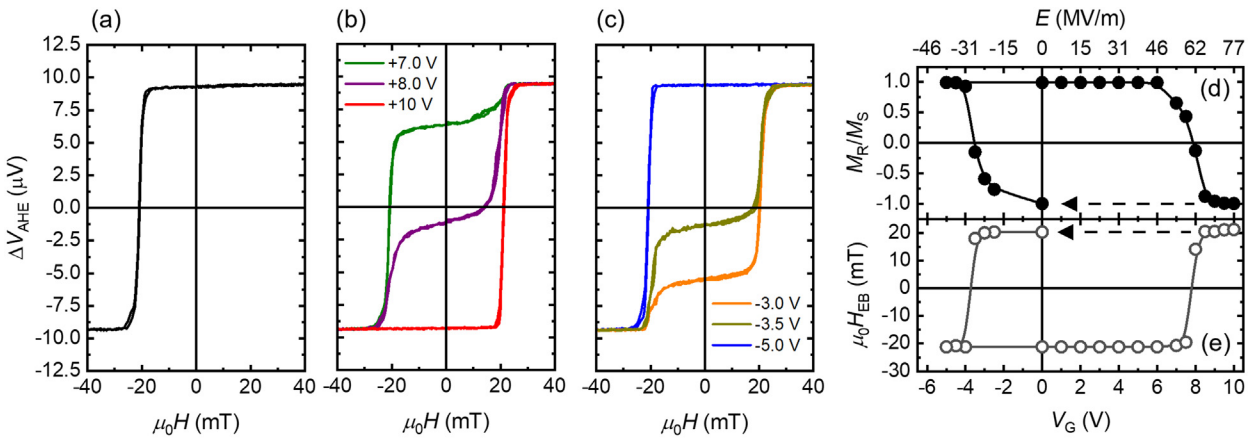

FIG. 5. (a) AHE loop just after the field cooling. (b) and (c) represent the AHE loops after applying V_G in combination with the high magnetic field (=5.5 T) in ascending and descending branches of V_G. V_G was +7.0 V (green), +8.0 (purple), and +10 V (red) for (b), and −3.0 V (orange), −3.5 V (dark yellow), and −5.0 V (blue) for (c). (d) and (e) represent the changes in M_R/M_S and $\mu_0 H_{EB}$ as a function of V_G, respectively. The top axis represents E calculated from V_G. Although the AHE signal was collected in ±500 mT, the enlarged curves ±40 mT are shown for the easy visibility of the switching field.

expression is derived based on the hypothesis that the AFM moments are pinned against the FM magnetization reversal. The second expression is derived from the AFM layer side. The ME switching of PEB is caused by the AFM domain switching.[20] In this process, the strong $\mu_0 H$ (= +5.5 T) was applied in combination with V_G, and it pins the FM moment during the AFM moment (the Néel vector) reversal. Based on the second expression, α is calculated to be 1.6 ps/m, very close to the reported value for the 500-nm thick Cr_2O_3 at $T/T_N = 0.97$–0.98.[36] This coincidence suggests that the Ir spacer layer transfers the ME-controlled AFM order parameter to the FM Pt/Co layer with no efficiency degradation.

In summary, we fabricated the epitaxial Pt/Co/Ir/Cr_2O_3/Pt film and investigated the magnetic/magnetoelectric properties. All studied films showed PMA. $\mu_0 H_C$ along the magnetic easy axis decreased by the insertion of the Ir spacer layer. For $t_{Ir} = 0.5$ nm, the lowest $\mu_0 H_C$ about 0.44 mT was obtained. The low H_C was maintained when the sample was cooled below T_N and PEB sets in. PEB with the low H_C could be switched in an isothermal way by applying V_G in combination with magnetic field. The switching of PEB showed the hysteresis as a function of V_G corresponding to the AFM domain switching. The hysteresis shifted along the V_G direction, and the analysis of the asymmetry provided α. The expected α is in good agreement with the reported value for the thick Cr_2O_3 film, suggesting no efficiency degradation of the ME properties. The results shown here indicate that the Ir spacer layer is a good candidate for the suppression of the H_C enhancement with PEB and as the spacer layer to transfer the ME-controlled AFM order parameter to the FM layer. It is known that the Pt/Co/Ir trilayer shows the strong interfacial DMI and the magnetic skyrmion can be formed.[37] The control of magnetic skyrmion motion has been so far demonstrated using electric current[38] and voltage.[39] The voltage control is especially promised for the low energy and fast operation, and the results shown here implies that the voltage control relying on the ME effect can be another root to control the skyrmion.

See the supplementary material for the magnetization curves, the temperature dependences of $\mu_0 H_{EB}$ and $\mu_0 H_C$ for the film with $t_{Ir} \geq 1.0$ nm, and the RHEED images for the film with the Pt spacer layer.

This work was partly supported by JSPS KAKENHI (Project Nos. 22H01757 and 22K18903), Iketani Science and Technology Foundation.

AUTHOR DECLARATIONS

Conflict of Interest

The authors have no conflicts to disclose.

Author Contributions

Hirofumi Ekawa: Data curation (equal); Formal analysis (equal); Writing – original draft (equal); Writing – review & editing (equal). **Jiaqi Shen:** Data curation (equal); Formal analysis (equal); Writing – review & editing (equal). **Kentaro Toyoki:** Data curation (equal); Methodology (equal); Writing – review & editing (equal). **Ryoichi Nakatani:** Supervision (equal); Writing – review & editing (equal). **Yu Shiratsuchi:** Conceptualization (lead); Data curation (equal); Formal analysis (equal); Funding acquisition (lead); Methodology (lead); Supervision (lead); Writing – original draft (lead); Writing – review & editing (lead).

DATA AVAILABILITY

The data that support the finding of this study are available from the corresponding author upon reasonable request.

REFERENCES

[1]S. Ikeda, J. Hayakawa, Y. M. Lee, F. Matsukura, Y. Ohno, T. Hanyu, and H. Ohno, IEEE Trans. Electron Devices **54**, 991 (2007).
[2]J. Nogués and I. K. Schuller, J. Magn. Magn. Mater. **192**, 203 (1999).
[3]A. E. Berkowitz and K. Takano, J. Magn. Magn. Mater. **200**, 552 (1999).
[4]K. Imakita, M. Tsunoda, and M. Takahashi, Appl. Phys. Lett. **85**, 3812 (2004).
[5]K. Liu, M. Baker, M. Tuominen, T. P. Russel, and I. K. Shuller, Phys. Rev. B **63**, 060403(R) (2001).
[6]H.-S. Song, K.-D. Lee, C.-Y. You, S.-H. Yang, S. Parkin, B.-G. Park, J.-W. Sohn, J.-I. Hong, and S.-C. Shin, Appl. Phys. Express **8**, 053002 (2015).
[7]B. Kocaman, K. Y. Aktaş, and A. C. Basaran, J. Magn. Magn. Mater. **530**, 167926 (2021).
[8]Y. Meng, J. Li, P.-A. Glans, C. A. Jenkins, E. Arenholz, A. Tan, J. Gibbons, J. S. Park, C. Hwang, H. W. Zhao, and Z. Q. Qiu, Phys. Rev. B **85**, 014425 (2012).
[9]Y.-J. Lee, C.-R. Chang, T.-M. Hong, C. H. Ho, and M.-T. Ling, J. Magn. Magn. Mater. **239**, 57 (2002).
[10]M. Tafur, W. Alayo, Y. T. Zhing, E. Baggio-Saitovitch, and V. P. Nascimento, J. Phys. D: Appl. Phys. **42**, 135001 (2009).
[11]N. J. Gökemeijer, T. Ambrose, and C. L. Chien, Phys. Rev. Lett. **79**, 4270 (1997).
[12]C. Pan, H. An, T. Harumoto, Z. Zhang, Y. Nakamura, and J. Shi, AIP Adv. **9**, 125046 (2019).
[13]F. Garcia, J. Sort, B. Rodmaq, A. Auffret, and B. Dieny, Appl. Phys. Lett. **83**, 3537 (2003).
[14]V. Baltz, A. Manchon, M. Tsoi, T. Moriyama, T. Ono, and Y. Tserkonvyak, Rev. Mod. Phys. **90**, 015005 (2018).
[15]X. He, Y. Wang, N. Wu, A. N. Caruso, E. Vescovo, K. D. Belashchenko, P. A. Dowben, and C. Binek, Nat. Mater. **9**, 579 (2010).
[16]T. Ashida, M. Oida, N. Shimomura, T. Nozaki, T. Shibata, and M. Sahashi, Appl. Phys. Lett. **106**, 132407 (2015).
[17]K. Toyoki, Y. Shiratsuchi, A. Kobane, C. Mitsumata, Y. Kotani, T. Nakamura, and R. Nakatani, Appl. Phys. Lett. **106**, 162404 (2015).
[18]Y. Shiratsuchi, T. Fujita, H. Oikawa, H. Noutomi, and R. Nakatani, Appl. Phys. Express **3**, 113001 (2010).
[19]M. Fiebig, J. Phys. D: Appl. Phys. **38**, R123 (2005).
[20]Y. Shiratsuchi, K. Toyoki, and R. Nakatani, J. Phys.: Condens. Matter **33**, 243001 (2021).
[21]T. V. A. Nguyen, Y. Shiratsuchi, A. Kobane, S. Yoshida, and R. Nakatani, J. Appl. Phys. **122**, 073905 (2017).
[22]T. V. A. Nguyen, Y. Shiratsuchi, S. Yonemura, T. Shibata, and R. Nakatani, J. Appl. Phys. **124**, 233902 (2018).
[23]Y. Shiratsuchi, T. Fujita, H. Noutomi, H. Oikawa, and R. Nakatani, IEEE Trans. Magn. **47**, 3909 (2011).
[24]Y. Shiratsuchi, W. Kuroda, T. V. A. Nguyen, Y. Kotani, K. Toyoki, T. Nakamura, M. Suzuki, K. Nakamura, and R. Nakatani, J. Appl. Phys. **121**, 073902 (2017).
[25]M. Suzuki, H. Muraoka, Y. Inaba, H. Miyagawa, N. Kawamura, T. Shimatsu, H. Maruyama, N. Ishimatsu, Y. Isohara, and Y. Sonobe, Phys. Rev. B **72**, 054430 (2005).
[26]Y.-C. Lau, Z. Chi, Y. Taniguchi, M. Kawaguchi, G. Shibata, N. Kawamura, M. Suzuki, S. Fukami, A. Fujimori, H. Ohno, and M. Hayashi, Phys. Rev. Mater. **3**, 104419 (2019).
[27]T. Koyama, A. Obinata, Y. Hibino, A. Hirohata, B. Kuerbanjiang, V. K. Lazarov, and D. Chiba, Appl. Phys. Lett. **106**, 132409 (2015).
[28]J. Wang, T. Seki, Y.-C. Lau, Y. K. Takahashi, and K. Takanashi, APL Mater. **9**, 061110 (2021).
[29]F. Wilheim, P. Pololoulus, H. Wende, A. Schez, L. Baberschhke, M. Angelekreis, N. K. Flevaris, and A. Rogalev, Phys. Rev. Lett. **87**, 207202 (2001).
[30]H. Ekawa, T. Okano, O. Huang, I. Iino, K. Toyoki, R. Nakatani, T. Kato, and Y. Shiratsuchi, Jpn. J. Appl. Phys. **62**, SB1002 (2023).
[31]M. Tsunoda, Y. Tsuchiya, T. Hashimoto, and M. Takahashi, J. Appl. Phys. **87**, 4375 (2000).

[32]K. O'Grady, L. E. Fernandez-Outon, and G. Vallejo-Fernandez, J. Magn. Magn. Mater. **322**, 883 (2010).
[33]J. Jia, Y. Chen, B. Wang, B. Han, Y. Wu, Y. Wang, and J. Cao, J. Phys. D: Appl. Phys. **52**, 065001 (2019).
[34]Y. Shiratsuchi, S. Yoshida, H. Yoshida, Y. Kotani, K. Toyoki, R. Nakatani, C. Mitsumata, and T. Nakamura, J. Appl. Phys. **127**, 153902 (2020).
[35]L. Liu, C. Zhou, T. Zhao, B. Yao, J. Zhou, X. Su, S. Chen, S. Shi, S. Xi, D. Lan, W. Lin, Q. Xie, L. Ren, Z. Luo, C. Shu, P. Yang, E.-J. Guo, Z. Dong, A. Manchon, and J. Chen, Nat. Commun. **13**, 3539 (2022).
[36]P. Borisov, T. Ashida, T. Nozaki, M. Sahashi, and D. Lederman, Phys. Rev. B **93**, 174415 (2016).
[37]C. Moreau-Luchaire, C. Moutafis, N. Reyren, J. Sampaio, C. A. F. Vaz, N. Van Horne, K. Bouzehouane, K. Garcia, C. Deranlot, P. Warnicke, P. Wohlhüter, J.-M. Goerge, M. Wiegand, J. Raabe, V. Cros, and A. Fert, Nat. Nanotechnol. **11**, 444 (2016).
[38]G. Yu, P. Opadhyaya, X. Li, S. K. Kim, Y. Fan, K. L. Wong, Y. Tserkovnyak, P. K. Amiri, and K. L. Wang, Nano Lett. **16**, 1981 (2016).
[39]T. Nozaki, Y. Jibiki, M. Goto, E. Tamura, T. Nozaki, H. Kubota, A. Fukushima, S. Yuasa, and Y. Suzuki, Appl. Phys. Lett. **114**, 012402 (2019).